UC Berkeley
UC Berkeley Previously Published Works

Title

Probing Metastable Domain Dynamics via Automated Experimentation in Piezoresponse Force Microscopy

Authors

Kelley, Kyle P
Ren, Yao
Dasgupta, Arvind
et al.

Peer reviewed

ARTICLE

Probing Metastable Domain Dynamics *via* Automated Experimentation in Piezoresponse Force Microscopy

Kyle P. Kelley,* Yao Ren, Arvind Dasgupta, Pravin Kavle, Stephen Jesse, Rama K. Vasudevan, Ye Cao, Lane W. Martin, and Sergei V. Kalinin*

Read Online

ACCESS | Metrics & More | Article Recommendations | Supporting Information

ABSTRACT: The dynamics of complex topological defects in ferroelectric materials is explored using automated experimentation in piezoresponse force microscopy. Specifically, a complex trigger system (*i.e.*, "FerroBot") is employed to study metastable domain-wall dynamics in $Pb_{0.6}Sr_{0.4}TiO_3$ thin films. Several regimes of superdomain wall dynamics have been identified, including smooth domain-wall motion and significant reconfiguration of the domain structures. We have further demonstrated that microscopic mechanisms of the domain-wall dynamics can be identified; *i.e.*, domain-wall bending can be separated from irreversible domain reconfiguration regimes. In conjunction, phase-field modeling was used to corroborate the observed mechanisms. As such, the observed superdomain dynamics can provide a model system for classical ferroelectric dynamics, much like how colloidal crystals provide a model system for atomic and molecular systems.

KEYWORDS: piezoresponse force microscopy, ferroelectric, domain-wall dynamics, automated experimentation, FerroBot, superdomain
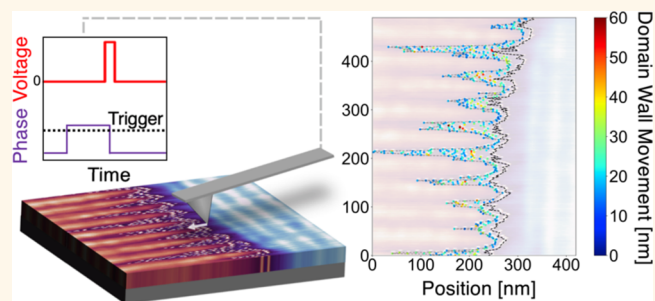
For over half a century, electromechanical and dielectric properties of ferroelectric materials have attracted the attention of applied and fundamental scientists alike.[1−4] Giant electromechanical responses in these materials have enabled a spectrum of applications in sensors and actuators, whereas the favorable dielectric properties underpin applications such as capacitors, tunable dielectric constant materials, *etc.* Similarly, the presence of switchable electrical polarization stimulated the development of a broad range of electronic device paradigms including ferroelectric field effect transistors,[5] nonvolatile memories,[4,6,7] domain-wall electronics,[8−11] and ferroelectric tunneling barrier[12−14] and multiferroic[15,16] devices.

Since the development of the thermodynamic theory of ferroelectrics, it has been realized that the functional properties of these materials emerge from the interplay of intrinsic material responses at the level of a single unit cell, and extrinsic contributions due to domain-wall dynamics.[1,17,18] The latter develop on the length scale of domain structures and can be large in magnitude, giving rise to strong size effects in ferroelectric thin films and devices.[2,19] Similarly, the introduction of structural disorder and close in energy symmetry-incompatible ground states in ferroelectric relaxors[20−22] and morphotropic[23−25] materials that increase the

density of domain walls and their mobility yields enhanced functionalities.

Understanding the role of domain walls in ferroelectric functionalities has given rise to the rapid growth of experimental and theoretical efforts in this direction. X-ray and neutron scattering have been used to explore the crystallographic changes with bias and time, providing insights into ferroelectric and ferroelastic domain-wall dynamics.[26,27] The development and broad propagation of piezoresponse force microscopy (PFM) and related spectroscopies have allowed visualization of ferroelectric domain structures on the sub-10 nm level,[28−32] leading to multiple observations of domain dynamics induced by the probe bias[33,34] or under the top electrode,[35] or induced by in-plane electric fields created by interdigitated electrodes.[36]
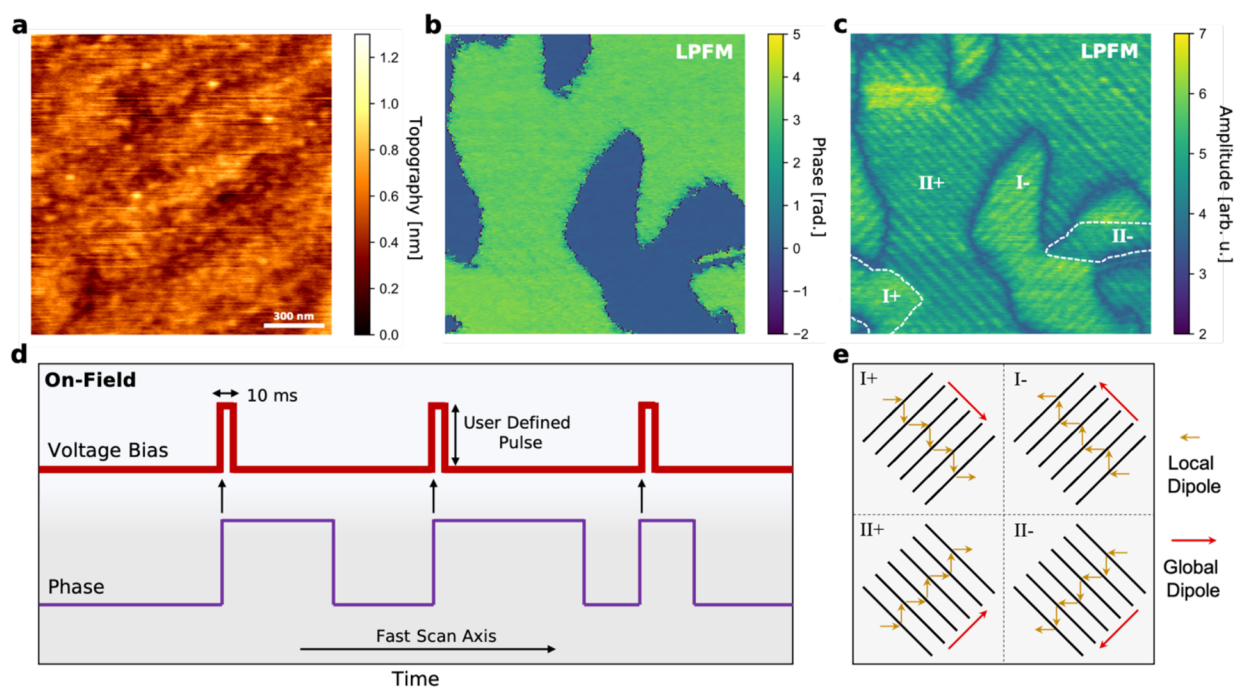
Figure 1. Lateral piezoresponse force microscopy of $Pb_{0.6}Sr_{0.4}TiO_3$ thin film. Representative (a) surface topography, single-frequency lateral piezoresponse force microscopy (b) phase, and (c) amplitude with four distinct ferroelectric in-plane domain orientations as illustrated in (e), and (d) FerroBot triggering scheme referred to as the on-field state.
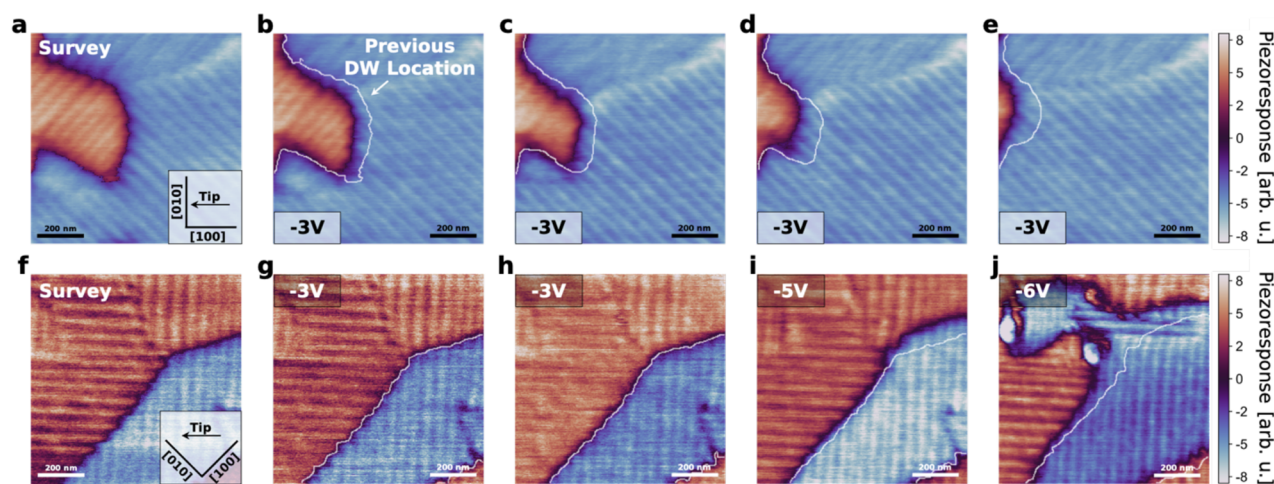

Figure 2. Domain wall motion dependence on tip-sample orientation. Lateral piezoresponse image of $Pb_{0.6}Sr_{0.4}TiO_3$ with fast scan axis (a) parallel to the [100] crystallographic direction (panel (a) inset) and corresponding images after executing FerroBot with (b−e) −3 V pulses (white lines indicate location of domain wall before pulsing). (f) Different location rotated 45° relative to [100] and [010] crystallographic directions (panel (f) inset) and corresponding images after executing FerroBot with (g, h) −3 V, (i) −5 V, and (j) −6 V pulses. Tip direction in the insets of panels (a) and (f) indicates fast-scan axis. Note the gradual motion of the domain wall for the top row, and strong pinning with subsequent nucleation-like switching and formation of disordered regions in the bottom row, suggesting fundamentally different wall motion mechanisms depending on relative orientation between tip motion direction and superdomain orientation.

However, observations of domain structure using PFM are generally limited to static domain configurations that evolve slowly on the time scale of the PFM image acquisition (~1−10 min). Several fast PFM studies have been reported;[37−39] however, these studies also rely on image-by-image observations. In another special case, mesoscale domain-wall dynamics were explored using spectroscopic imaging in PFM, enabled by strong pinning *via* unbiased wall segments[40] or existing structural defects.[41−43] However, generally, the studies of

dynamic-wall behavior away from (meta)stable equilibrium are limited.

RESULTS AND DISCUSSION

Here, we demonstrate that automated experiments (AE) in PFM can be used to explore the dynamic regimes of wall dynamics. We extend the previously reported line-by-line detection system (FerroBOT[44]) toward exploring the dynamics of domain walls in dense *a-c* superdomain (or domain-bundle)[45,46] systems and demonstrate that this approach can
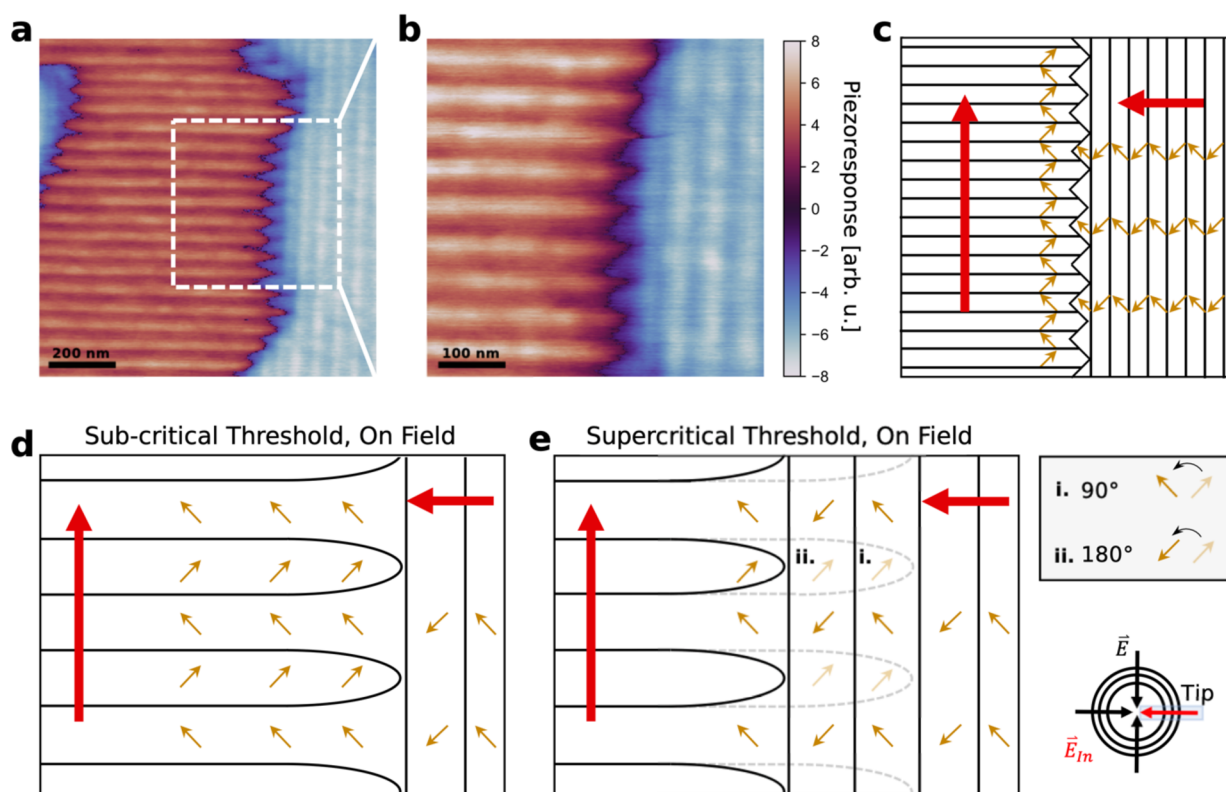
Figure 3. Local response of domain wall with FerroBOT. Piezoresponse images with (a) zig-zagged vertical domain wall and (b) zoomed area of interest. (c) Schematic illustrating local and global dipole orientations. (d, e) Illustration of domain wall bending at sub-critical and supercritical voltages for domain wall motion. Note, subpanels in (e) correspond to dipole orientations (gray box) and electric field at tip.

be used to explore both reversible (wall bending) and irreversible (superdomain reorientation) transformation mechanisms.

As a model system, we investigate superstructure domain-wall dynamics in $Pb_{0.6}Sr_{0.4}TiO_3$ thin films (Methods/Experimental Section). Representative surface topography (Figure 1a) reveals a smooth sample for scanning probe-based experiments. The ferroelectric behavior is investigated *via* single-frequency PFM - lateral phase and amplitude images shown (Figure 1b,c, respectively). As such, the clear superstructure can be observed with two orthogonal orientations for each phase, as outlined by the white dotted lines and labels (I-, I+, II-, and II+ in Figure 1c). Correspondingly, the domain orientations are illustrated (Figure 1e), displaying the local and global dipoles as gold and red, respectively. As such, the local gold arrows indicate the dipoles within the specific orientations, while the red arrows indicate the global polarization vector, consistent with previous reports.[47]

To probe the domain-wall dynamics, we implement AE using the FerroBot framework, as described previously.[44] Briefly, the detected signal during PFM scanning is passed to a logic circuit that detects a specific local event underneath the AFM probe, such as the crossing of a domain wall or a more complex descriptor. Upon detection of the event, FerroBot can be configured to produce a user-defined set of actions, such as generating a voltage pulse, light pulse, or mechanical stimulus. Here, we use a single-frequency PFM phase as the detector for in-plane domain walls and apply 10 ms voltage pulses only at the domain wall defined by a negative phase change (Figure 1d, negative to positive piezoresponse). Further, we vary the voltage pulse from −2.5 V to −7.5 V to identify the threshold

for domain-wall motion. It should be mentioned that this technique can be employed using a number of feedbacks (*e.g.*, current, amplitude, topography, *etc.*) on a variety of platforms coupled with varying stimuli. Using this AE method, the characteristics and metastability of a defined domain-wall type can be explored, gaining rich insight into switching behavior in complex ferroelectric systems.

First, we aimed to explore the dynamic phenomena in the dense ferroelastic domain structures by applying defined voltage pulses at superdomain walls (negative to positive phase transition) for two orientations: (i) 45° and (ii) 0°/90° relative to the slow scan axis. With the tip fast-scan axis parallel to the [100] direction, −3 V pulses result in a monotonic decrease in the red domain, clearly observed by the domain-wall moving to the left (Figure 2b−e). In stark contrast, when the superstructure is rotated by 45°, −3 V pulses seemingly have little or no effect on moving the domain wall (Figure 2g,h). However, upon increasing the pulse magnitude to −5 V (Figure 2i), motion is observed on the upper portion of the blue domain. Further increasing the pulse magnitude results in a burst of the blue-domain orientation with regions of frustration (Figure 2j, bright blue regions). Interestingly, the blue domain's onset of growth occurs at the intersection of the two orientations with the same phase (red), indicating the presence of a potentially metastable region.

As shown (Figure 2g−j), the domain-wall motion is severely impeded when applying voltage pulses while the tip motion is either parallel or perpendicular to the domain wall, as opposed to the case where the tip motion is at 45° to the wall. Moreover, the energy threshold for domain-wall motion is clearly higher for this configuration, and when the domain wall
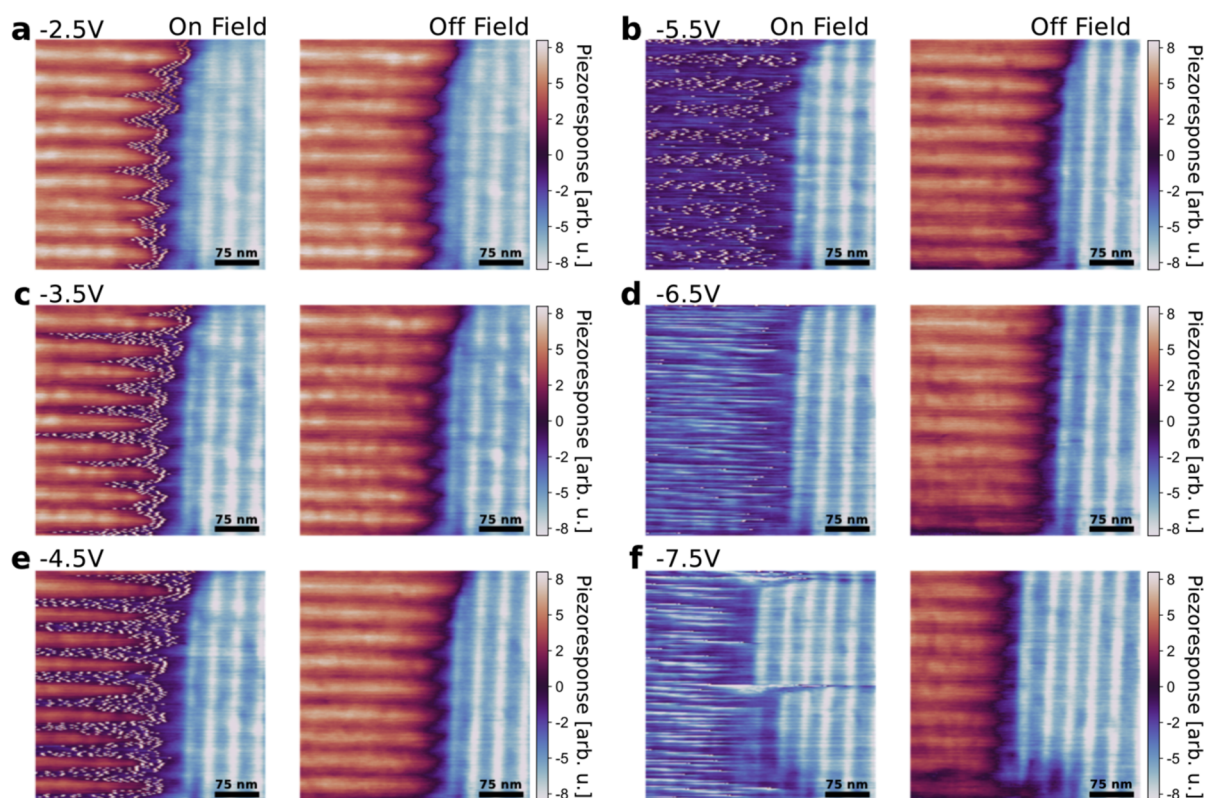
Figure 4. Domain wall motion bias magnitude dependence. Piezoresponse images of on-field (left panel) and off-field (right panel) with (a, c, e) sub-critical voltage pulses (−2.5, −3.5, and −4.5 V pulse, respectively), and (b, d, f) supercritical super voltage pulses (−5.5, −6.5, and −7.5 V, respectively).
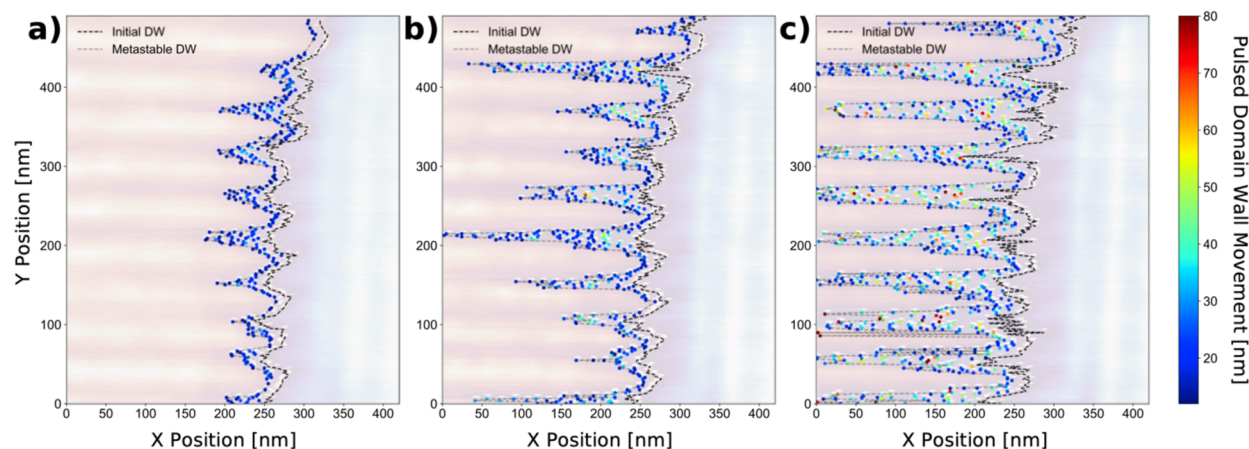

Figure 5. Pulsed domain wall spatial analysis. On-field FerroBOT piezoresponse images with pulse magnitudes of (a) −2.5 V, (b) −3.5 V, and (c) −4.5 V analyzed for domain-wall motion per pulse. Superimposed scatter plot indicates the detected location of the domain wall after the previous pulse was applied with the color scale indicating length of travel. Black dotted and gray dotted lines indicate initial domain wall location and final, metastable domain wall location, respectively.

does move, it does so in an erratic and seemingly uncontrollable fashion. It appears as if, when the in-plane electric field created during simultaneously pulsing and scanning aligns with the global polarization (Figure 2a−e), the domain wall moves under smaller bias in a controllable manner. However, when the in-plane electric field is aligned with the local polarization (Figure 2f−j), i.e., individual a-domains, the polarization switching becomes unstable and forces reconstructions. Here, understanding and controlling how the domain wall moves is a critical factor in the fundamental understanding of in-plane polarization switching, and more importantly, it is detrimental

in developing strategies for creating specific domain-wall configurations ultimately underpinning a broad range of applications.

As such, to further understand the mechanisms by which the global domain walls move, we focus on a localized region consisting of a vertical domain wall with an imbedded zigzag like structure (Figure 3a,b). As shown (Figure 3c), the two phases have distinct dipole orientations, which give rise to the observed domain structure. We aim to explore the mechanisms of the wall dynamic between these structures that give rise to the phenomena in Figure 2f−j.
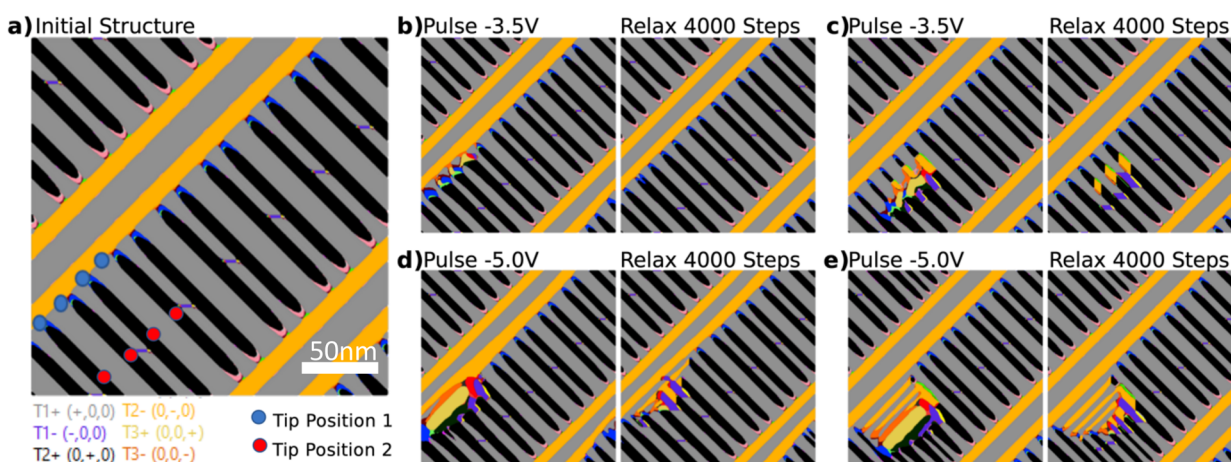
Figure 6. Phase-field simulation results. The domain structures of (a) initial state. (b−e) applying a pulse (left panel) of (b, c) −3.5 V and (d, e) −5 V and relaxing for 4000 steps (right panel). Tip groups are placed at two different locations as indicated in the initial structure with red/blue circles. The (b, d) structures are from tip position 1 (blue circle), while (c, e) are from tip position 2 (red circle).

Figure 4 shows the systematic increase in pulse magnitude for both the on-field (during pulsing) and off-field (*i.e.*, traditional single-frequency PFM scanning) for voltage pulses spanning −2.5 V to −7.5 V. For the on-field FerroBOT images, white pixels can be clearly observed corresponding to the pulsing locations. Briefly, as the 10 ms voltage pulse is applied, the electrostatic contribution to the cantilever response is affected, producing a small artifact, in this case, the small white pixels seen in the on-field. To our advantage, the pulsing induced artifacts allow us to confirm where the pulses are being applied. Moreover, these artifacts enable further domain-wall dynamics to be derived. For voltage pulses spanning −2.5 V and −4.5 V, a snap-back like dynamic effect can be observed (Figure 4a,c,e), which becomes progressively larger with pulse magnitude. Moreover, this snap-back region is larger for one domain orientation, *versus* the other. Presumably, the local dipoles on both sides of this domain wall have the same orientations, ultimately enabling preferential domain-wall motion as illustrated in Figure 4a,c,e. In contrast, applying voltage pulses larger than −5.5 V results in irreversible domain-wall motion (Figure 4b,d,f).

Next, we examined the distance of domain-wall travel in the snap-back region, *i.e.*, with −2.5, −3.5, and −4.5 V pulses. Specifically, the location of each pulse is identified *via* bright spots (Figure 4, on-field) and the distance between the subsequent pulses is calculated, yielding the distance the domain wall travels per pulse. The results are illustrated (Figure 5) where the superimposed scatter plots indicate the magnitude of domain-wall motion. Under −2.5 V pulses (Figure 5a), the metastable domain wall moves uniformly with an average distance of 18.7 ± 4.3 nm. In contrast, applying a −3.5 V pulse results in substantial metastable domain-wall motion with the top 10% of distances averaging 42.4 ± 7.8 nm, all located within the domains with the lower energy barrier. Interestingly, the average distance the entire domain wall travels during the last pulse is 19.6 ± 5.5 nm, similar to the −2.5 V pulses, suggesting a similar barrier is present when the domain wall experiences significant bending. A similar behavior is observed for −4.5 V pulses with the top 10% of domain-wall motion averaging 70.0 ± 27.2 nm.

To explain these observations, we propose that, by increasing the pulsing density along the domain wall of interest (for 0°/90° relative orientations), two regimes of domain-wall motion occur. Below a certain threshold, the inner local domains with the same dipole orientation move with strong bending occurring at the domain wall formed at the opposing dipole orientation (Figure 3d). Upon increasing the pulse magnitude above the threshold, significant motion and bending of the local domain wall will cause the extended domain to collapse, forming a pair of vertical domains (Figure 3e). Correspondingly, one would expect the formed vertical domains to undergo 90° and 180° polarization rotations to minimize electrostatic energy.

To gain further insight in these mechanisms, we performed phase-field simulations of the superstructure where voltage pulses are applied in a similar fashion. As shown (Figure 6a), an initial structure consisting of global dipole II+ and II- is constructed and fully relaxed under a tensile strain of 3%. To mimic the motion of the tip at the domain boundary, four tips of 15 nm radius are grouped together and placed at two positions as indicated (Figure 6a). At tip position 1, when a pulse of −3.5 V is applied, some mixed domains are formed near the domain boundary near the tip location along the domain boundary (Figure 6b). After the bias is turned off, the domain structure eventually relaxes to its initial state, which is quite similar to the snap-back phenomenon under the sub-critical pulse voltages. In contrast, increasing the pulse to −5 V leads to the formation of a pair of global domain II+ inside the previous region of II-, similar to that under supercritical voltages (Figure 6d). This global domain II+ is stable and does not disappear even after the removal of the tip bias. It is noteworthy that the domain-wall bending seems to also exist in the local domain (T_1+/T_2+). To verify this bending effect, the tip group is placed at tip position 2. Under −3.5 V, it is seen that that a stronger bending occurs at the domain wall of global dipole II+ and II- than tip position 1 (Figure 6c). The domain-wall bending results in a thinner local T_2+ domain (black, Figure 6c) than that in the initial structure. Moreover, increasing the voltage to −5.0 V at tip position 2 also results in pairs of irreversible global domain II+ due to the stronger domain-wall bending (Figure 6e). Thus, our phase-field simulations agree well with the experimental observations. It is also important to note that the close matching between the phase-field predictions and the experimentally observed voltage intervals suggests that experimentally realized conditions are close to that in the phase-field model, including the absence of

significant extrinsic pinning. This in turn suggests that the phase-field models can be used not only for qualitative but also quantitative descriptions of domain-wall dynamics in complex structures.

CONCLUSION

To summarize, here we have explored the dynamics of the domain walls between superdomain bundles in polydomain ferroelectric materials using an AE approach. Several regimes of superdomain wall dynamics have been identified, including smooth domain-wall motion and phase transitions associated with the significant reconfiguration of domain structures. We have further demonstrated that microscopic mechanisms of the domain-wall dynamics can be explored, identified, and separated from the wall bending and irreversible domain reconfiguration regimes. More generally, we illustrate that AE in PFM is a powerful tool for the exploration of the dynamic and static properties of domain walls and other topological defects in systems with the complex microstructures. We believe that this approach will both stimulate the emergence of predictive phase-field models and provide a framework for their verification and will ultimately broadly usher automated experimentation into the field of ferroelectrics and scanning probe microscopy.

METHODS/EXPERIMENTAL SECTION

Materials. The films studied in this work were produced with pulsed-laser deposition using a KrF excimer laser (248 nm, LPX 300, Coherent). The work here focuses on heterostructures of the form 100 nm $Pb_{0.6}Sr_{0.4}TiO_3$/30 nm $SrRuO_3$/$DyScO_3$ (110) (CrysTec GmbH). The $Pb_{0.6}Sr_{0.4}TiO_3$ growth was carried out at a heater temperature of 625 °C in a dynamic oxygen pressure of 200 mTorr with a laser fluence of 1.9 J/cm². The laser repetition rates of 10 and 2 Hz were used for the $Pb_{1.1}TiO_3$ ceramic target (Praxair) and the $SrTiO_3$ single crystal target, respectively. The desired composition was achieved *via* subunit cell-level material mixing using the synchronized targets motion and laser pulse sequence. The 10% excess lead in the $Pb_{1.1}TiO_3$ target was found to be vital to compensate the lead loss during growth. The $SrRuO_3$ growth was carried out at a heater temperature of 690 °C in a dynamic oxygen pressure of 100 mTorr with a laser fluence of 1 J/cm² and a laser repetition rate of 17 Hz from a ceramic target (Praxair) of the same composition. Following the growth, the samples were cooled to room temperature at 10 °C/min in a static oxygen pressure of 700 Torr. The as-grown films were also characterized by X-ray diffraction including symmetric θ-2θ line scans, rocking curves, and 2D reciprocal space mapping (RSM) studies using a high-resolution X-ray diffraction (XRD) X'pert Pro2, PANalytical system (see Supporting Information Figure S1). All films studied herein were found to be highly crystalline and fully epitaxial.

Instrumentation. FerroBot measurements were employed *via* an Oxford Instruments Asylum Research Cypher atomic force microscopy modified for real-time manipulation. Signal processing and real time domain manipulation were driven by a coupled National Instruments USB-7856R multifunctional RIO and Stanford Research Systems RF lock-in amplifier (model SR844). Specifically, FerroBot was set to trigger under a negative to positive phase switch, resulting in a user-defined voltage pulse being applied to the AFM tip. All experiments used Budget Sensor Multi75E-G Cr/Pt coated AFM probes (~3 N/m).

Phase-Field Simulation. In the phase-field simulation, we choose $PbTiO_3$ as our model system. This is because the simulated equilibrium domain structure using energy coefficients of $PbTiO_3$ yield the best agreement with the experiments.[48] The polarization vector $P_i = (P_x, P_y, P_z)$ is employed as the order parameter to describe the ferroelectric state in the ferroelectric thin film. The temporal evolution of P_i is determined by minimizing the total free energy (F)

with respect to P_i *via* numerically solving the time-dependent Landau−Ginzburg−Devonshire (LGD) equations[49]

$$\frac{\partial P_i(x, t)}{\partial t} = -L \frac{\delta F}{\delta P_i(x, t)}, \; (i = 1 \sim 3) \tag{1}$$

where x is the spatial position, t is time, and L is the kinetic coefficient related to the domain-wall mobility. The total free energy of the thin film includes the Landau, gradient, elastic, and electrostatic energies, which can be written as

$$F = \int_V [f_{lan}(P_i) + f_{grad}(P_{i,j}) + f_{elas}(P_i, \varepsilon_{ij}) + f_{elec}(P_i, E_i)] dV \tag{2}$$

where V is the total volume of the system, and ε_{ij} and E_i are the components of strain and electric fields. Detailed expression of each free energy density in eq 2 can be found in the literature.[48] Equation 1 is numerically solved by a semi-implicit spectral method.[50] The total simulation system is chosen to be $256\Delta x \times 256\Delta y \times 32\Delta z$, with $\Delta x = \Delta y = \Delta z = 1.0$ nm. The thicknesses of the film, the substrate, and the air are set to be $20\Delta z$, $10\Delta z$, and $2\Delta z$, respectively. The temperature is 25 °C, and an isotropic relative dielectric constant (κ_{ii}) is chosen to be 50. The gradient energy coefficients are set to be $G_{11}/G_{110} = 0.6$, while $G_{110} = 1.73 \times 10^{-10}$ $C^{-2}m^4N$. The substrate strain is set to be 3% to keep the global II+/II- structure stable. The Landau coefficients, electrostrictive coefficients, and elastic-compliance constants are collected from ref 48.

To simulate the effect of a local scanning probe tip, we define the electrical potential distribution[51] induced by the tip group on the top surface of the ferroelectric thin film as

$$\phi(x, y) = \sum_{i=1}^{4} \phi_0 \frac{\gamma^2}{(x - x_i)^2 + (y - y_i)^2 + \gamma^2} \tag{3}$$

in which ϕ_0 is the tip bias, (x_i, y_i) is the position of the *i*th tip in the tip group, 4 means 4 tips in the tip group, and γ is the half-width half magnitude of the tip. Here, we choose $\gamma = 15$ nm together with the tip group to mimic the scanning process of the tip on the domain boundary. The ferroelectric thin film is grounded on the bottom surface.

ASSOCIATED CONTENT

ⓢ Supporting Information

The Supporting Information is available free of charge at https://pubs.acs.org/doi/10.1021/acsnano.1c05455.

> Additional information including X-ray diffraction, piezoresponse force microscopy images *versus* sample orientation, and vertical piezoresponse force microscopy images (PDF)

AUTHOR INFORMATION

Corresponding Authors

Kyle P. Kelley − *The Center for Nanophase Materials Sciences, Oak Ridge National Laboratory, Oak Ridge, Tennessee 37831, United States;* ⦿ orcid.org/0000-0002-7688-0484; Email: kelleykp@ornl.gov

Sergei V. Kalinin − *The Center for Nanophase Materials Sciences, Oak Ridge National Laboratory, Oak Ridge, Tennessee 37831, United States;* ⦿ orcid.org/0000-0001-5354-6152; Email: sergei2@ornl.gov

Authors

Yao Ren − *Department of Materials Science and Engineering, University of Texas at Arlington, Arlington, Texas 76019, United States*

Arvind Dasgupta − *Department of Materials Science and Engineering, University of California Berkeley, Berkeley, California 94720, United States*

Pravin Kavle − *Department of Materials Science and Engineering, University of California Berkeley, Berkeley, California 94720, United States*

Stephen Jesse − *The Center for Nanophase Materials Sciences, Oak Ridge National Laboratory, Oak Ridge, Tennessee 37831, United States*

Rama K. Vasudevan − *The Center for Nanophase Materials Sciences, Oak Ridge National Laboratory, Oak Ridge, Tennessee 37831, United States;* ⊙ orcid.org/0000-0003-4692-8579

Ye Cao − *Department of Materials Science and Engineering, University of Texas at Arlington, Arlington, Texas 76019, United States;* ⊙ orcid.org/0000-0002-7365-7447

Lane W. Martin − *Department of Materials Science and Engineering, University of California Berkeley, Berkeley, California 94720, United States; Materials Sciences Division, Lawrence Berkeley National Laboratory, Berkeley, California 94720, United States*

Complete contact information is available at:
https://pubs.acs.org/10.1021/acsnano.1c05455

Notes

ACKNOWLEDGMENTS

REFERENCES

(1) Tagantsev, A. K.; Cross, L. E.; Fousek, J. *Domains in Ferroic Crystals and Thin Films*; Springer: New York, 2010.

(2) Shaw, T. M.; Trolier-McKinstry, S.; McIntyre, P. C. The Properties of Ferroelectric Films at Small Dimensions. *Annu. Rev. Mater. Sci.* **2000**, *30*, 263−298.

(3) Scott, J. F. Applications of Modern Ferroelectrics. *Science* **2007**, *315* (5814), 954−959.

(4) Ha, S. D.; Ramanathan, S. Adaptive Oxide Electronics: A Review. *J. Appl. Phys.* **2011**, *110* (7), 071101.

(5) Miller, S. L.; McWhorter, P. J. Physics of the Ferroelectric Nonvolatile Memory Field-Effect Transistor. *J. Appl. Phys.* **1992**, *72* (12), 5999−6010.

(6) Dearaujo, C. A. P.; Cuchiaro, J. D.; McMillan, L. D.; Scott, M. C.; Scott, J. F. Fatigue-Free Ferroelectric Capacitors with Platinum-Electrodes. *Nature* **1995**, *374* (6523), 627−629.

(7) Scott, J. F.; Paz de Araujo, C. A. Ferroelectric Memories. *Science* **1989**, *246* (4936), 1400−1405.

(8) Catalan, G.; Seidel, J.; Ramesh, R.; Scott, J. F. Domain Wall Nanoelectronics. *Rev. Mod. Phys.* **2012**, *84* (1), 119−156.

(9) Seidel, J.; Martin, L. W.; He, Q.; Zhan, Q.; Chu, Y. H.; Rother, A.; Hawkridge, M. E.; Maksymovych, P.; Yu, P.; Gajek, M.; Balke, N.; Kalinin, S. V.; Gemming, S.; Wang, F.; Catalan, G.; Scott, J. F.; Spaldin, N. A.; Orenstein, J.; Ramesh, R. Conduction at Domain Walls in Oxide Multiferroics. *Nat. Mater.* **2009**, *8* (3), 229−234.

(10) Guyonnet, J.; Gaponenko, I.; Gariglio, S.; Paruch, P. Conduction at Domain Walls in Insulating Pb(Zr0.2ti0.8)O3 Thin Films. *Adv. Mater.* **2011**, *23* (45), 5377−5382.

(11) Vasudevan, R. K.; Wu, W. D.; Guest, J. R.; Baddorf, A. P.; Morozovska, A. N.; Eliseev, E. A.; Balke, N.; Nagarajan, V.; Maksymovych, P.; Kalinin, S. V. Domain Wall Conduction and Polarization-Mediated Transport in Ferroelectrics. *Adv. Funct. Mater.* **2013**, *23* (20), 2592−2616.

(12) Tsymbal, E. Y.; Kohlstedt, H. Applied Physics - Tunneling across a Ferroelectric. *Science* **2006**, *313* (5784), 181−183.

(13) Gruverman, A.; Wu, D.; Lu, H.; Wang, Y.; Jang, H. W.; Folkman, C. M.; Zhuravlev, M. Y.; Felker, D.; Rzchowski, M.; Eom, C. B.; Tsymbal, E. Y. Tunneling Electroresistance Effect in Ferroelectric Tunnel Junctions at the Nanoscale. *Nano Lett.* **2009**, *9* (10), 3539−3543.

(14) Maksymovych, P.; Jesse, S.; Yu, P.; Ramesh, R.; Baddorf, A. P.; Kalinin, S. V. Polarization Control of Electron Tunneling into Ferroelectric Surfaces. *Science* **2009**, *324* (5933), 1421−1425.

(15) Garcia, V.; Bibes, M.; Bocher, L.; Valencia, S.; Kronast, F.; Crassous, A.; Moya, X.; Enouz-Vedrenne, S.; Gloter, A.; Imhoff, D.; Deranlot, C.; Mathur, N. D.; Fusil, S.; Bouzehouane, K.; Barthelemy, A. Ferroelectric Control of Spin Polarization. *Science* **2010**, *327* (5969), 1106−1110.

(16) Bibes, M.; Villegas, J. E.; Barthelemy, A. Ultrathin Oxide Films and Interfaces for Electronics and Spintronics. *Adv. Phys.* **2011**, *60* (1), 5−84.

(17) Damjanovic, D. Ferroelectric, Dielectric and Piezoelectric Properties of Ferroelectric Thin Films and Ceramics. *Rep. Prog. Phys.* **1998**, *61* (9), 1267−1324.

(18) Damjanovic, D. Stress and Frequency Dependence of the Direct Piezoelectric Effect in Ferroelectric Ceramics. *J. Appl. Phys.* **1997**, *82* (4), 1788−1797.

(19) Bintachitt, P.; Jesse, S.; Damjanovic, D.; Han, Y.; Reaney, I. M.; Trolier-McKinstry, S.; Kalinin, S. V. Collective Dynamics Underpins Rayleigh Behavior in Disordered Polycrystalline Ferroelectrics. *Proc. Natl. Acad. Sci. U. S. A.* **2010**, *107* (16), 7219−7224.

(20) Tagantsev, A. K.; Glazounov, A. E. Does Freezing in Pbmg1/3nb2/3o3 Relaxor Manifest Itself in Nonlinear Dielectric Susceptibility? *Appl. Appl. Phys. Lett.* **1999**, *74* (13), 1910−1912.

(21) Glazounov, A. E.; Tagantsev, A. K. Direct Evidence for Vogel-Fulcher Freezing in Relaxor Ferroelectrics. *Appl. Phys. Lett.* **1998**, *73* (6), 856−858.

(22) Shvartsman, V.; Tyunina, A.; Levoska, J.; Kholkin, A. Local Electromechanical Properties of Pbmg1/3nb2/3o3 Thin Films Studied by Piezoelectric Force Microscopy. *Ferroelectrics* **2004**, *302* (1), 323−326.

(23) Woodward, D. I.; Knudsen, J.; Reaney, I. M. Review of Crystal and Domain Structures in the $PbZr_xTi_{1-x}O_3$ Solid Solution. *Phys. Rev. B: Condens. Matter Mater. Phys.* **2005**, *72* (10), 104110.

(24) Zeches, R. J.; Rossell, M. D.; Zhang, J. X.; Hatt, A. J.; He, Q.; Yang, C. H.; Kumar, A.; Wang, C. H.; Melville, A.; Adamo, C.; Sheng, G.; Chu, Y. H.; Ihlefeld, J. F.; Erni, R.; Ederer, C.; Gopalan, V.; Chen, L. Q.; Schlom, D. G.; Spaldin, N. A.; Martin, L. W.; et al. A Strain-

Driven Morphotropic Phase Boundary in Bifeo(3). *Science* **2009**, *326* (5955), 977−980.

(25) Zhang, J. X.; Xiang, B.; He, Q.; Seidel, J.; Zeches, R. J.; Yu, P.; Yang, S. Y.; Wang, C. H.; Chu, Y. H.; Martin, L. W.; Minor, A. M.; Ramesh, R. Large Field-Induced Strains in a Lead-Free Piezoelectric Material. *Nat. Nanotechnol.* **2011**, *6* (2), 98−102.

(26) Jones, J. L.; Slamovich, E. B.; Bowman, K. J. Domain Texture Distributions in Tetragonal Lead Zirconate Titanate by X-Ray and Neutron Diffraction. *J. Appl. Phys.* **2005**, *97* (3), 034113.

(27) Jones, J. L.; Hoffman, M.; Daniels, J. E.; Studer, A. J. Direct Measurement of the Domain Switching Contribution to the Dynamic Piezoelectric Response in Ferroelectric Ceramics. *Appl. Phys. Lett.* **2006**, *89* (9), 092901.

(28) Kolosov, O.; Gruverman, A.; Hatano, J.; Takahashi, K.; Tokumoto, H. Nanoscale Visualization and Control of Ferroelectric Domains by Atomic-Force Microscopy. *Phys. Rev. Lett.* **1995**, *74* (21), 4309−4312.

(29) Franke, K.; Besold, J.; Haessler, W.; Seegebarth, C. Modification and Detection of Domains on Ferroelectric Pzt Films by Scanning Force Microscopy. *Surf. Sci.* **1994**, *302* (1−2), L283−L288.

(30) Franke, K.; Weihnacht, M. Evaluation of Electrically Polar Substances by Electric Scanning Force Microscopy 0.1. Measurement Signals Due to Maxwell Stress. *Ferroelectr., Lett. Sect.* **1995**, *19* (1−2), 25−33.

(31) Hong, J. W.; Park, S. I.; Khim, Z. G. Measurement of Hardness, Surface Potential, and Charge Distribution with Dynamic Contact Mode Electrostatic Force Microscope. *Rev. Sci. Instrum.* **1999**, *70* (3), 1735−1739.

(32) Takata, K.; Kushida, K.; Torii, K. Strain-Imaging Observation of Pb(Zr,Ti)O-3 Thin-Films. *Japanese Journal of Applied Physics Part 1-Regular Papers Short Notes & Review Papers* **1995**, *34* (5B), 2890−2894.

(33) Gruverman, A.; Kalinin, S. V. Piezoresponse Force Microscopy and Recent Advances in Nanoscale Studies of Ferroelectrics. *J. Mater. Sci.* **2006**, *41* (1), 107−116.

(34) Gruverman, A.; Auciello, O.; Ramesh, R.; Tokumoto, H. Scanning Force Microscopy of Domain Structure in Ferroelectric Thin Films: Imaging and Control. *Nanotechnology* **1997**, *8*, A38−A43.

(35) Gruverman, A.; Kholkin, A. Nanoscale Ferroelectrics: Processing, Characterization and Future Trends. *Rep. Prog. Phys.* **2006**, *69* (8), 2443−2474.

(36) Balke, N.; Gajek, M.; Tagantsev, A. K.; Martin, L. W.; Chu, Y. H.; Ramesh, R.; Kalinin, S. V. Direct Observation of Capacitor Switching Using Planar Electrodes. *Adv. Funct. Mater.* **2010**, *20* (20), 3466−3475.

(37) Nath, R.; Chu, Y. H.; Polomoff, N. A.; Ramesh, R.; Huey, B. D. High Speed Piezoresponse Force Microscopy: < 1 Frame Per Second Nanoscale Imaging. *Appl. Phys. Lett.* **2008**, *93* (7), 072905.

(38) Polomoff, N. A.; Premnath, R. N.; Bosse, J. L.; Huey, B. D. Ferroelectric Domain Switching Dynamics with Combined 20 Nm and 10 Ns Resolution. *J. Mater. Sci.* **2009**, *44* (19), 5189−5196.

(39) Steffes, J. J.; Ristau, R. A.; Ramesh, R.; Huey, B. D. Thickness Scaling of Ferroelectricity in Bifeo3 by Tomographic Atomic Force Microscopy. *Proc. Natl. Acad. Sci. U. S. A.* **2019**, *116* (7), 2413−2418.

(40) Aravind, V. R.; Morozovska, A. N.; Bhattacharyya, S.; Lee, D.; Jesse, S.; Grinberg, I.; Li, Y. L.; Choudhury, S.; Wu, P.; Seal, K.; Rappe, A. M.; Svechnikov, S. V.; Eliseev, E. A.; Phillpot, S. R.; Chen, L. Q.; Gopalan, V.; Kalinin, S. V. Correlated Polarization Switching in the Proximity of a 180 Degrees Domain Wall. *Phys. Rev. B: Condens. Matter Mater. Phys.* **2010**, *82* (2), 024111.

(41) Rodriguez, B. J.; Chu, Y. H.; Ramesh, R.; Kalinin, S. V. Ferroelectric Domain Wall Pinning at a Bicrystal Grain Boundary in Bismuth Ferrite. *Appl. Phys. Lett.* **2008**, *93* (14), 142901.

(42) Kalinin, S. V.; Jesse, S.; Rodriguez, B. J.; Chu, Y. H.; Ramesh, R.; Eliseev, E. A.; Morozovska, A. N. Probing the Role of Single Defects on the Thermodynamics of Electric-Field Induced Phase Transitions. *Phys. Rev. Lett.* **2008**, *100* (15), 155703.

(43) Rodriguez, B. J.; Choudhury, S.; Chu, Y. H.; Bhattacharyya, A.; Jesse, S.; Seal, K.; Baddorf, A. P.; Ramesh, R.; Chen, L. Q.; Kalinin, S. V. Unraveling Deterministic Mesoscopic Polarization Switching Mechanisms: Spatially Resolved Studies of a Tilt Grain Boundary in Bismuth Ferrite. *Adv. Funct. Mater.* **2009**, *19* (13), 2053−2063.

(44) Kelley, K. P.; Ren, Y.; Morozovska, A. N.; Eliseev, E. A.; Ehara, Y.; Funakubo, H.; Giamarchi, T.; Balke, N.; Vasudevan, R. K.; Cao, Y.; Jesse, S.; Kalinin, S. V. Dynamic Manipulation in Piezoresponse Force Microscopy: Creating Nonequilibrium Phases with Large Electromechanical Response. *ACS Nano* **2020**, *14* (8), 10569−10577.

(45) Wicks, S.; Seal, K.; Jesse, S.; Anbusathaiah, V.; Leach, S.; Garcia, R. E.; Kalinin, S. V.; Nagarajan, V. Collective Dynamics in Nanostructured Polycrystalline Ferroelectric Thin Films Using Local Time-Resolved Measurements and Switching Spectroscopy. *Acta Mater.* **2010**, *58* (1), 67−75.

(46) Ivry, Y.; Chu, D. P.; Scott, J. F.; Durkan, C. Flux Closure Vortexlike Domain Structures in Ferroelectric Thin Films. *Phys. Rev. Lett.* **2010**, *104* (20), 207602.

(47) Matzen, S.; Nesterov, O.; Rispens, G.; Heuver, J. A.; Biegalski, M.; Christen, H. M.; Noheda, B. Super Switching and Control of In-Plane Ferroelectric Nanodomains in Strained Thin Films. *Nat. Commun.* **2014**, *5*, 4415.

(48) Haun, M. J.; Furman, E.; Jang, S. J.; Mckinstry, H. A.; Cross, L. E. Thermodynamic Theory of Pbtio3. *J. Appl. Phys.* **1987**, *62* (8), 3331−3338.

(49) Chen, L. Q. Phase-Field Method of Phase Transitions/Domain Structures in Ferroelectric Thin Films: A Review. *J. Am. Ceram. Soc.* **2008**, *91* (6), 1835−1844.

(50) Chen, L. Q.; Shen, J. Applications of Semi-Implicit Fourier-Spectral Method to Phase Field Equations. *Comput. Phys. Commun.* **1998**, *108* (2−3), 147−158.

(51) Choudhury, S.; Zhang, J. X.; Li, Y. L.; Chen, L. Q.; Jia, Q. X.; Kalinin, S. V. Effect of Ferroelastic Twin Walls on Local Polarization Switching: Phase-Field Modeling. *Appl. Phys. Lett.* **2008**, *93* (16), 162901.